Rheo-Optical Investigation of Wormlike Polymers in Solution

Yiannis Gatzonis, Sanaul K. Siddiquee, and Jan W. van Egmond*

Department of Chemical Engineering, University of Massachusetts, Amherst, Massachusetts 01003

Received December 17, 1996; Revised Manuscript Received September 2, 1997[⊗]

ABSTRACT: The rheo-optical response of semidilute solutions of monodisperse, wormlike poly(*n*-hexyl isocyanate) (PHIC) in simple shear flow was investigated using a flow birefringence technique. The optical equivalent of viscosity η_b as measured by birefringence was found to depend on the contour length L, concentration c, and the ratio of contour length to persistence length L/α. The power exponent of the concentration dependence of viscosity increased with increasing L/α with $\eta_b \sim c^{3.2}$ for $L/\alpha \cong 0.8$, $\eta_b \sim c^{4.0}$ for $L/\alpha \cong 1.8$, and $\eta_b \sim c^{4.2}$ for $L/\alpha \cong 3.3$. A simple scaling relation for viscosity, $\eta \sim c^4 L^{-3} L_e^8$, where L_e is the effective rigid rod length of the wormlike chain and is a function of L/α, is derived for the regime $L \cong \alpha$ and substantiated experimentally. Further, PHIC solutions at concentrations below 6% exhibited two well separated relaxation modes after flow cessation. While the fast mode is attributed to molecular reorientation, dynamic light scattering confirms that the slow mode may be attributed to the formation of large multichain structures.

Introduction

The low-frequency dynamic and rheological behavior of polymers in semidilute solution is governed by the effect of entanglements on the chain diffusion. This behavior is reasonably well described theoretically for flexible[1−4] and rigid rod[3,5] polymers. For example, as described in theories by Doi and Edwards, both flexible and rigid polymers are assumed to reptate through confining tubes comprised of their neighbors.[3] Theoretically and experimentally, however, dynamic properties such as viscosity and relaxation times are strongly dependent on chain stiffness. For example, difficulties are encountered in the study of rod reptation because polymers usually regarded as rodlike display a degree of flexibility as expressed by their persistence length α, relative to their contour length L. On the basis of relaxation of a rodlike molecule from a tube, Keep and Pecora[6] have shown that flexibility can become an important factor in the dynamics of rodlike molecules in semidilute solution even when $L/\alpha = 0.1$. Hence, polymers such as poly(γ-benzyl L-glutamate) (PBLG), for which $\alpha \cong 100$ nm, are sometimes better described as wormlike chains at the molecular weights typically studied.[7,8] Increasing interest has been shown in the rheological properties of wormlike polymers.[9−13] Recently the original reptation and tube theories have been extended to include the effect of flexibility.[9−11] Further, Sato *et al.*[12] have introduced the "fuzzy cylinder" model that accounts for the entanglement effects by treating a wormlike polymer as a cylinder on the basis that the local conformational dynamics are much faster than global motions. However, studies on the dynamics and rheology of semidilute wormlike polymers relative to those on flexible polymers are scarce, limited primarily to PBLG,[14] xanthan,[15−17] sodium hyaluronate,[18,19] polyisocyanates,[20] and polyelectrolytes.[21] A broad consensus on the rheology of entangled wormlike chains is therefore still elusive.

This paper investigates the dynamics of wormlike chains by probing the rheo-optical response of poly(*n*-hexyl isocyanate) (PHIC). This choice of PHIC was made because (1) it has been a useful model polymer to test theories of dilute wormlike chains and is therefore well characterized;[6,22−25] and (2) monodisperse samples of PHIC were readily available. The dilute solution properties of PHIC have previously been studied by light scattering,[6,23,26,27] viscometry,[22−24,28−30] and dielectric dispersion methods.[31] Chain rigidity is a consequence of its helical configuration caused by a competition between electronic and steric factors.[28] Torsional degrees of freedom account for limited chain flexibility and have been included in a general helical wormlike chain model developed by Yamakawa and co-workers.[32] Various studies on PHIC show that as L/α is increased, the chain undergoes a gradual conformational change from rodlike to coillike.[33−36]

Dynamic properties are highly dependent on contour length, and therefore polydispersity can be a serious problem. This is especially pronounced for semidilute solutions of rodlike polymers, where the viscosity scales as $L^{6.3}$. Either corrections are made to account for polydispersity[37,38] or fractionated samples are used.[22−25,27,28,39] The PHIC samples used in this investigation were provided by Professor Novak's group at the University of Massachusetts. This synthesis technique involves an organotitanium(IV)-based living polymerization of isocyanates which provides strict control over the molecular weight and polydispersity of the sample.[40]

A complication in the rheology of PHIC solutions is the possible formation of intermolecular associations. There are many experimental reports that suggest that a large variety of rodlike polymers form aggregates in various solvents. In static light-scattering experiments an increase in the intensity at low angles is observed; and in dynamic light scattering (DLS), one or more slow modes appears.[41−45] Both these observations have been interpreted as being due to the formation of large length scale multichain structures. This phenomenon has been observed in rodlike polyelectrolytes such as xanthan[46] and short DNA chains[34,41−43] but also in nonionic polymers.[6,44,45] The exact mechanism of cluster formation is still not well understood. Odijk has recently shown that the long-range attractive force between polyelectrolyte molecules may rationalize the onset of aggregation of rodlike DNA chains.[47] For nonionic polymers, van der Waals attractions probably play an important role in aggregation. Slow modes have also been observed by DLS in polyelectrolyte solutions for a

[⊗] Abstract published in *Advance ACS Abstracts,* November 1, 1997.

S0024-9297(96)01854-2 CCC: $14.00

wide variety of synthetic structures.[48−52] The characteristic time of the slow mode is typically several orders of magnitude greater than that of the fast mode and increases with dilution. In recent studies, Sedlak[50,52] concluded that poor solvation is not the reason for domain formation in solutions of polyelectrolytes.

There is evidence that poly(alkyl isocyanates) also form aggregates. Electric birefringence decay and dielectric relaxation studies of PHIC solutions in toluene indicate the presence of at least one slow mode.[39] From DLS measurements, Keep and Pecora[6] found slow modes in certain PHIC solutions in cyclohexane. These slow modes dominated the depolarized scattering and corresponded to a hydrodynamic radius of several microns. In both the above studies, low solubility may have contributed to the slow mode.

The viscosity of polyisocyanate solutions has previously been studied by Aharoni,[53] Aharoni and Wang,[54] and Ohshima *et al.*[20] using mechanical techniques. In the present study, we use a birefringence technique to measure the optical equivalent of viscosity η_b in semidilute solution. Since birefringence depends on molecular alignment rather than bulk mechanical properties, birefringence provides an appropriate test for molecular theories. By using samples with different molecular weights, we investigate the effect of chain conformation on rheological properties. Further, birefringence can also be used to detect molecular associations. Slow modes possibly associated with aggregation are observed by flow birefringence and dynamic light scattering.

Theory

As the polymer concentration increases, chains progressively interpenetrate and their dynamics become affected by topological constraints. This effect becomes evident when the average distance between the centers of mass of the chains is equal to the average chain extension, which for rods is at the concentration $\nu > 1/L^3$, where $\nu = (\rho/M)N_A$ is the number of polymers per unit volume. At higher concentrations, when $\nu > 1/bL2$ (where b is the chain diameter), excluded volume becomes important and rod alignment becomes dependent on alignment of neighboring rods. In a series of articles, Doi and Edwards[55] developed a model describing the dynamics of rigid rod polymers. In the semidilute regime ($1/L^3 < \nu < 1/bL^2$) motion parallel to the rod orientation is unrestricted, while lateral motion is severely restricted by surrounding rods. This restricted motion can be represented by diffusion of the rod parallel to its contour in a tube that is composed of surrounding rods. The tube diameter $a' \cong 1/\nu L^2$ depends on polymer concentration, average orientation, and length. Rod dynamics depend on the disengagement time $\tau_d = L^2/D_{||}$, where $D_{||} \cong L^2 D_{r0}$ is the parallel diffusion coefficient and $D_{r0} = 3k_BT/(\pi\eta_s L^3)\ \ln(L/b)$ is the dilute rotational diffusion coefficient. Since the time for the rod to become disoriented by disengagement from successive tubes is $\tau_d(L/a')^2$, D_r is given by the expression

$$D_r = D_{r0}\left(\frac{a'}{L}\right)^2 = D_{r0}\beta(\nu L^3)^{-2} \sim c^{-2}M^{-7} \qquad (1)$$

where β is a numerical factor. Hence, D_r and the characteristic rheological time, $\tau = 1/(6D_r)$, can be predicted from dilute data.

The stress tensor σ_{ij} for a semidilute solution of rods can be written as the sum of a viscous and an elastic contribution[3]

$$\sigma_{ij} = 3\nu k_BT(\langle u_i u_j\rangle - \delta_{ij}/3) + \nu\zeta\langle u_i u_j u_k u_l\rangle D_{kl} \qquad (2)$$

where $\mathbf{u}$ is the unit vector characterizing molecular orientation, ζ is the friction coefficient, and D_{ij} is the rate of strain of the imposed flow. In eq 2, the first term on the right hand side corresponds to the elastic contribution to the stress, while the second term is the viscous term. It has been argued[3,4] that $\zeta \cong k_BT/D_{r0} = 6k_BT\tau(\nu L^3)^{-2}$. Hence, in the semidilute regime, as long as the shear rate $\dot\gamma$ is much smaller than $1/\tau$, the stress is only due to the elastic contribution and the viscosity $\eta \sim \nu\tau$ is given by[3]

$$\nu = \frac{\pi}{30\beta}\eta_s\frac{(\nu L^3)^3}{\ln(L/b)} \sim c^3M^6 \qquad (3)$$

Furthermore, the stress is proportional to the conformation tensor $\langle\mathbf{uu}\rangle$, and hence the stress−optic rule holds and viscosity can be measured by a birefringence technique.[56]

The above relations have been derived for rods ($L \ll \alpha$). However, the flexibility of a rodlike molecule should affect its rotational motion because the end of the molecule will be more free to choose its direction when translating out of a tube even though the molecular orientation may be restricted along the rest of its length. For partially flexible chains ($L \approx \alpha$) Doi[10] and Semenov[11] have developed theories to account for chain bending motion during chain reptation. Since considerable bending motion can occur during the time τ_d that the molecule disengages from the tube, dynamic properties should be affected by flexibility through the ratio L/α. Doi[10] has suggested that if bending motions occur quickly, the motion may be time-averaged, resulting in the polymer behaving as a rigid rod with an effective length L_e. If the contour length is not too high, an estimation of the length L_e can be made from the average chain length projected on the central segment of a Kratky−Porod chain,[10]

$$L_e = 2\alpha(1 - e^{-L/2\alpha}) \qquad (4)$$

Another approach based on a "fuzzy cylinder" model[12] is to use the root mean squared end-to-end distance $\langle R^2\rangle^{1/2}$ for the effective length. An estimate of the concentration for crossover to the semidilute regime of the shorter 'effective' rods is $c^* \sim L_e^{-2}$, which is in agreement with the experimental observations[7,8] on solutions of stiff polymers with $L/\alpha \sim 1$ that entanglement effects start at concentrations much greater than $c^* \sim L^{-2}$. Semenov[11] has argued that if $\nu \ll 1/L\alpha^2$, persistent segments of length α can move freely, since the mean number of such segments is small in a volume α^3. By this logic, the crossover concentration is given as $c^* \sim \alpha^{-2} \sim L_e^{-2}$ for $L/\alpha \sim 1$. The relation $c^* \sim \alpha^{-2}$ can also be obtained from the concentration at which the concentration-dependent correlation length ξ is equal to the Kuhn length (2α).[15] Further, the disengagement time $\tau_d = L_e^2/D_{||}$ is shortened by an amount L_e^2/L^2 to within a logarithmic correction. To estimate the diffusion coefficient, each chain is divided into almost rectilinear parts of length α. It will be assumed that friction is only due to solvent viscosity and that the friction coefficient for the whole chain is then the sum of the friction coefficients for these rodlike parts. Then, to within a logarithmic correction,[11]

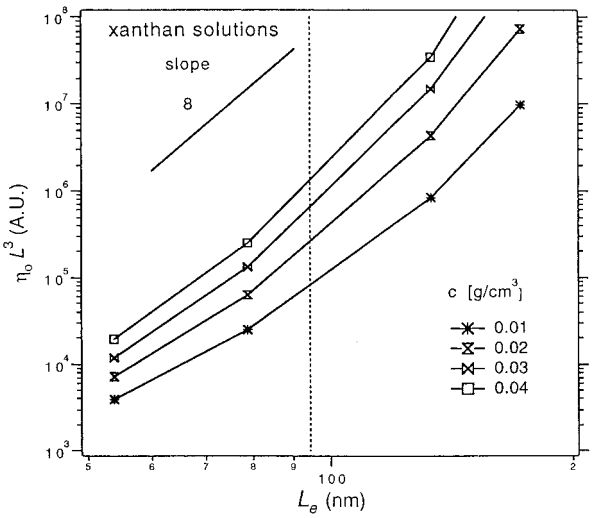

Figure 1. Dependence of ηL^3 (in arbitrary units) vs effective length L_e for aqueous xanthan at the indicated concentrations (data obtained from ref 17): dashed line indicates $L_e = 94.5$ nm for $L = \alpha = 120$ nm. A line with slope = 8 is included for comparison to the data.

$$D_{\parallel} = \frac{k_B T \ln(\alpha/b)}{2\pi\eta_s L} \tag{5}$$

As noted by Doi,[10] the estimation of the tube diameter a' when $L \cong \alpha$ is difficult. For rigid rods, $a' \sim \nu^{-1} L^{-2}$. For stiff chains undergoing rapid bending fluctuations, the length of the rod is replaced by the effective length and Doi[10] estimated $\alpha' \sim \nu^{-1} L_e^{-2}$. But since bending fluctuations cause the chains contributing to the topological constraints to effectively occupy a greater average volume over a time scale less than the disengagement time, we speculate that the effective tube diameter contracts and $a' \sim \nu^{-\delta} L_e^{-2}$, where $\delta \geq 1$. The rotational diffusion coefficient D_r is then given by eq 1

$$D_r = \frac{1}{\tau_d}\left(\frac{a'}{L_e}\right)^2 = D_{\parallel}\frac{\beta}{L_e^{\,2}}(\nu^{\delta} L_e^{\,3})^{-2} \sim \nu^{-2\delta} L^{-1} L_e^{\,-8} \tag{6}$$

Consequently the rotational diffusion coefficient increases by a factor of $(L/L_e)^8$ as a result of flexibility. Imposing the scaling relation $\eta = \eta_s f(c/c^*)$ and using the condition in eq 6 that $\eta \sim \nu/D_r \sim L_e^{\,8}$ and $c^* \sim L_e^{-2}$, we obtain $\eta \sim \eta_s(c/c^*)^4 \sim c^4$. Since $\delta = {}^3/_2$, which corresponds to tube diameter contraction by bending fluctuations,

$$\eta = \frac{\nu}{D_r} \sim \nu^4 L L_e^{\,8} \sim c^4 L^{-3} L_e^{\,8} \tag{7}$$

For $L \cong L_e$, eq 7 then suggests $\tau \sim c^3 M^6$.

Using dynamic light scattering for semidilute PBLG with $L/\alpha \cong 1$, Zero and Pecora[7] observed the scaling $\tau \sim 1/D_r \sim M^{5.6\pm0.6}$. On the other hand, using electric birefringence relaxation measurements in semidilute PBLG with $L/\alpha \cong 1$ Mori *et al.*[8] reported $\tau \sim cM^5$. Detailed studies on the viscosity of semidilute xanthan solutions by Takada *et al.*[17] have shown that the slope of the logarithmic plot of η vs c increases from 3 for $L/\alpha = 0.5$ to approximately 7 for $L/\alpha = 10$. We have displayed the data of Takada *et al.* for various concentrations on a logarithmic plot of ηL^3 vs L_e (Figure 1). For the effective chain length, the projection definition proposed by Doi (eq 4) was applied. As can be seen, the slopes of the plots are approximately 8 when $L = \alpha = 120$ nm (i.e. $L_e = 94.5$ nm), consistent with our scaling relation proposed in eq 7. A more comprehensive theory based on the fuzzy cylinder model[12] for chains with $L/\alpha < 10$ gives predictions that agree with the viscosity data of Takada *et al.*[17] for xanthan solutions. Longer wormlike molecules have also been studied. For semidilute hyaluronate solutions ($L/\alpha \cong 100$), Fouissac *et al.*[18] found $\eta_{spo} \sim c^{4.0\pm0.2} M^4$, which corresponds to the same scaling relation proposed by de Gennes[57] for linear flexible polymers interacting by topological entanglements but without hydrodynamic or excluded volume interactions. This is essentially consistent with the open structure of very long wormlike polymers with $L \gg \alpha \gg b$. Although hyaluronate is a polyelectrolyte, the effect of long range electrostatic interactions was screened out by the addition of 0.1 M NaCl.

Table 1. Sample Characterization

PHIC	M_w	PDI	L/α
P15	15 390	1.061	0.8
P34	33 750	1.117	1.8
P62	62 240	1.299	3.3

Table 2. Persistence Length Dependence on Solvent Polarity

solvent	dielectric constant	polarity μ_{solv} (D)	persistence length[a] (nm)
hexane	1.89	0.0	42
toluene	2.568	0.36	40
chloroform	4.806	1.01	30[b]
TCE	8.20	1.32	20−30[c]
DCM	8.925	1.60	20

[a] Information is from reference 36. [b] Persistence length for poly(*n*-butyl isocyanate). [c] Estimated.

Experimental Section

Materials. Three PHIC samples of molecular weights $M_w = 15\,000$, $M_w = 34\,000$, and $M_w = 62\,000$ referred to as samples P15, P34, and P62, respectively, were synthesized by living polymerization. The samples were characterized using a tandem GPC/LS, and relatively low polydispersities were recorded (Table 1). Normal GPC (relative to monodisperse polystyrene standards) gives erroneous results of high polydispersity ($M_w/M_n > 20$). This indicates that separation of these polymers is not based strictly on size exclusion but may involve another phenomenon based on an affinity of these polymers for the GPC column substrate.[58] Polydispersity increased with increasing molecular weight due to the longer reaction times needed to obtain appreciable yields of the higher molecular weight polymer.

There is an unusual solvent dependence of the global dimension of PHIC that suggests a general decrease in polymer dimensions with increasing solvent polarity. This dependence was first discovered by Schneider *et al.*[59] and was investigated in greater depth using intrinsic viscometry measurements by Berger and Tidswell.[28] The decrease in persistence length with increasing solvent dipole moment μ_{solv} can be seen in Table 2 (information was obtained from Cook *et al.*[36]). NMR line-width measurements indicate that there is an additional interaction between the solvent dipole moment and the chain backbone that allows for larger torsional oscillations and thus smaller chain dimensions in polar solvents.[36]

Tetrachloroethane (TCE) is an excellent solvent for rheological experiments on PHIC due to its relatively high viscosity and boiling point. On the basis of the dependence of α on μ_{solv} in Table 2, the persistence

length of PHIC in TCE ($\mu_{solv} = 1.32$ D) was estimated to be in the range $\alpha = 20-30$ nm. The monomer projection length of PHIC is 0.2 nm,[28] while the molecular weight of a monomer unit is 127. Assuming a contour length of $\alpha = 30$ nm, which corresponds to a chain segment with $M_w = 19\,000$, the ratio L/α is presented in Table 1 for each of the samples. The hard-core diameter b as determined by intrinsic viscosity measurements[24] and light scattering techniques[35] is approximately 1.6 nm. Due to their larger size, interactions between wormlike polymers become more important at much lower concentrations than those for flexible polymers and the rheological behavior is controlled by the degree of chain overlapping. Solutions ranging in concentration from 2 to 15 wt% were prepared. Replacing the rod length L with the effective length L_e, the overlap concentration c^* can be calculated. In the case of polymer P34, the semidilute regime occurs at $c > 0.03$ g/cm^3.

The rheological time scale may be estimated from the rotational diffusion coefficient given by eq 6. For the samples considered in this study, 0.1 ms $< \tau <$ 10 ms. As a result, shear thinning is not expected for the shear rates applied as $\tau\dot{\gamma} < 1$. Furthermore, no overshoots in start-up of shear flow are expected, and it is expected that the first normal stress relative to the shear stress will be negligible. Consequently, the steady state angle of birefringence should be at 45° to the flow axis for all but the highest molecular weight polymers.

Rheo-Optics. Birefringence was used to measure the dynamics of chain orientation and extension. In anisotropic polymeric media, the refractive index tensor **n** is proportional to the averaged segmental conformation tensor $\langle \mathbf{rr} \rangle$, where **r** is the segment vector. The birefringence $\Delta n'$ is the degree of anisotropy along the principal axis of $\langle \mathbf{rr} \rangle$ rotated at an angle χ to the flow direction. Since the probing beam passed through the gap between the cylinders in the flow cell along the vorticity axis, the average monomer orientation and degree of orientation were measured in the plane of the velocity and velocity gradient. The flow birefringence technique utilized a standard setup.[56] A He−Ne laser provided monochromatic light at 632 nm. A polarization state generator (PSG) consisting of a linear polarizer and a rotating half wave plate was placed before the sample, while a circular polarizer was placed after the flow cell. The transmitted intensity recorded at the detector is then given as

$$\frac{I}{I_0/2} = 1 - \sin\delta' \sin 2\chi \cos 4\omega t + \sin\delta' \cos 2\chi \sin 4\omega t \quad (8)$$

where I_0 is the intensity of the light incident on the PSG, δ' and χ are the retardance and orientation angle with respect to the flow direction, respectively, and ω is the frequency of the rotating half wave plate. The oscillating intensity at the detector can be separated into out-of-phase and in-phase components, $R_1 = -\sin\delta' \sin 2\chi$ and $R_2 = \sin\delta' \cos 2\chi$, respectively. The retardance and orientation angle were determined from these two components as follows

$$\chi = \frac{1}{2}\arctan\left(\frac{-R_1}{R_2}\right), \quad \delta' = \arcsin(R_1^2 + R_2^2)^{1/2} \quad (9)$$

The birefringence $\Delta n'$ is related to the retardance δ':

$$\Delta n' \equiv \delta'\lambda/(2\pi d) \quad (10)$$

where d is the path length of the light beam in the sample. Since the stress−optic rule is expected to hold for shear rates with $\dot{\gamma} < 1/\tau$,[4] the birefringence and the angle of birefringence can be used to obtain the shear stress σ_{xy} and the first normal stress difference N_1,

$$\sigma_{xy} = \frac{n_{xy}}{C} = \frac{\Delta n'}{2C}\sin 2\chi \quad \text{and} \quad N_1 = \frac{n_{xx} - n_{yy}}{C} = \frac{\Delta n'}{C}\cos 2\chi \quad (11)$$

where C is the stress−optic coefficient and $n_{\alpha\beta}$ is the $\alpha\beta$-component of the refractive index tensor. The optical equivalent of the viscosity is determined from the shear component, i.e. $\eta_b = n_{xy}/\dot{\gamma}$. The entire experiment including the shear rate applied to the cell, data collection, and data analysis was computer-controlled. A more detailed description of the instruments, the optical elements, and the analysis can be found in ref 56 and 60.

Flow Cell. All the experiments were performed at room temperature (21 °C) using a Couette flow cell consisting of two concentric cylinders. The gap width between the cylinders ($h = 3$ mm) is much smaller than the diameter of the cylinders (18 mm for the outer cylinder), ensuring a good approximation to homogeneous shear flow. The height of the cup—i.e. the path length of the laser beam through the solution—was 19 mm. For concentrations of 15% and above, the attenuation was so large that the beam intensity was not strong enough to register in the photodiode. This large amount of scattering resulted from the proximity to the biphasic liquid crystal/isotropic system. Applied shear rates varied from 5 to 250 s^{-1}. To reduce noise, experimental data presented in this paper represent averages over 10−30 identical runs.

Dynamic Light Scattering. For the DLS experiments, solutions of concentration 2.00, 1.00, 0.50, and 0.25 wt % were prepared and allowed to equilibrate for 1 or 2 days. Samples were filtered through a 0.5 μm Millipore filter into a dust-free scattering cell. The temperature in the cell was maintained at 25 °C with a toluene bath.

The DLS measurements were performed on a spectrometer consisting of an automatic ALV goniometer and an ALV 5000 correlator. For the light source, a linearly polarized Ar ion laser (Coherent Laser) at the $\lambda_0 = 514.5$ nm line was used. The normalized intensity time correlation function $g_2(q,t) = \langle I(q,t)\, I(q,0)\rangle/\langle |I(q,0)|^2\rangle$, where $I(q,0)$ is the scattered intensity, was measured in the 'multi-τ' mode over the time range 10^{-4} to 10^4 ms. The wavenumber is given by $q = (4\pi n/\lambda_0)\sin(\theta/2)$, where n is the solution refractive index and θ is the probing angle. Measurements were taken in the angular range from 30° to 120° at 15° intervals.

If the scattered light follows Gaussian statistics, $g_2(t)$ is given by the Siegert relation[61]

$$g_2(t) = 1 + \beta|g_1(t)|^2 \quad (12)$$

where $g_1(q,t) = \langle E(q,t)\, E^*(q,0)\rangle/\langle |E(q,0)|^2\rangle$ is the normalized electric field autocorrelation function and β is an apparatus-dependent factor. Since the continuous decay time distribution $w(\tau)$ is unknown and possibly broad or multimodal, CONTIN[62] was the preferred method of analysis. This method assumes that $g_1(t)$ is

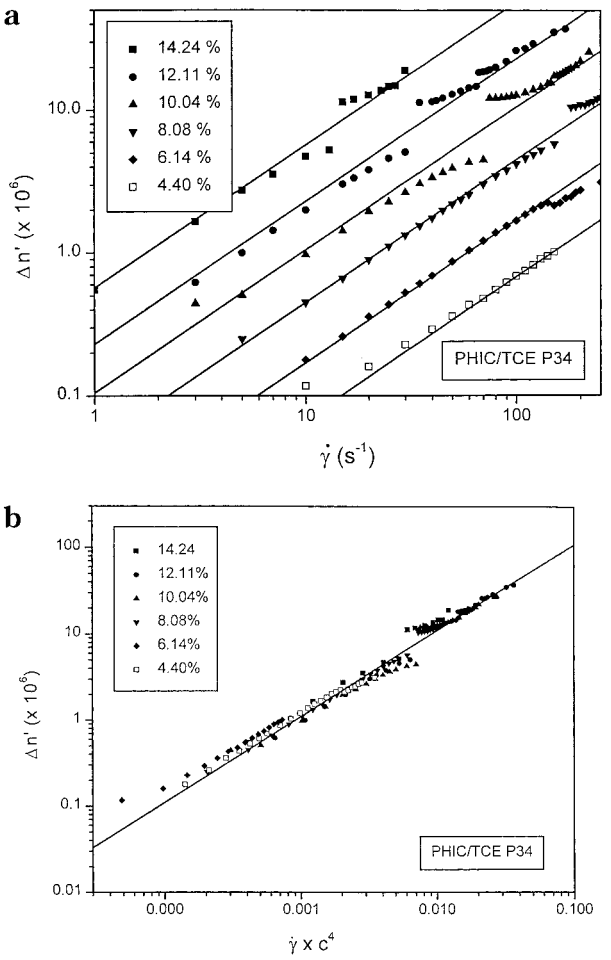

Figure 2. (a) Steady state birefringence $\Delta n'$ vs shear rate for P34. (b) Steady state birefringence vs $\dot{\gamma}c^4$.

represented by

$$g_1(t) = \int_0^\infty w(\tau) \exp(-t/\tau)\, d\tau \qquad (13)$$

By fitting correlation curves with CONTIN, the characteristic decay times τ of the relaxation distribution were evaluated.

Results and Discussion

Simple shear experiments were performed on solutions of PHIC samples P15, P34, and P62 with concentrations varying from 2% to 15% by weight.

Steady State Birefringence. Figure 2a shows the steady state birefringence as a function of shear rate for the P34 (M_w = 34 000) solutions at various concentrations. The birefringence is positive and increases linearly as shear rate is increased. The steady state birefringence data collapsed into a single line (Figure 2b) after the shear rate was rescaled with concentration to the fourth power, i.e. $n_{xy}/\dot{\gamma} \sim c^4$. Furthermore, this observed scaling relation was independent of shear rate, indicating that there was no shear-thinning at the shear rates investigated. For sample P62, the 6% and 8% steady state birefringence data followed the scaling relation $n_{xy}/\dot{\gamma} \sim c^{4.2}$, while solutions of P15 followed $n_{xy}/\dot{\gamma} \sim c^{3.2}$ (Figure 3).

Flow birefringence arises from the orientation of the polymer chains in a shear field, and as a result of the stress−optic rule,[56] we expect the steady state birefringence divided by shear rate and viscosity to exhibit the same dependence on concentration. Indeed, the steady state birefringence dependence on concentration $n_{xy}/\dot{\gamma} \sim c^{3.2}$ observed for the nearly rodlike P15 sample ($L/\alpha = 0.8$) is close to the viscosity dependence on concentration predicted by Doi and Edwards[55] and observed by Chow and Fuller[37] for rigid rods, $\eta \sim c^3$. The relation $\eta \sim c^4$ exhibited by the P34 solutions is consistent with our predicted scaling relation in eq 7. For sample P62 the concentration dependence of viscosity exhibited an exponent of 4.2. Thus, as L/α increases, the concentration exponent increases from 3 to values greater than 4. For wormlike chains, it has been predicted[57] and observed[18,19] that $\eta \sim c^4$ as $L/\alpha \to \infty$. Hence, there ought to be a value of L/α at which the exponent reaches a maximum value. To test our scaling relation (eq 7), we have displayed ηL^3 vs L_e calculated with α = 30 nm for various concentrations on a logarithmic plot (Figure 4). As can be seen, in the vicinity of L_e = 23.6 nm (corresponding to $L = \alpha$), the slopes of the plots are approximately 8, as expected.

The retardation δ', which is related to the birefringence according to eq 10, "goes over orders" when it exceeds a value of $\pi/2$. Since the instrument measures $\sin(\delta')$ (see eq 8), the calculation of birefringence becomes ambiguous when retardance is near $\delta' = \pi/2, 3\pi/2, 5\pi/2$, etc. This is the reason for the small gaps observed in the steady state birefringence data in Figure

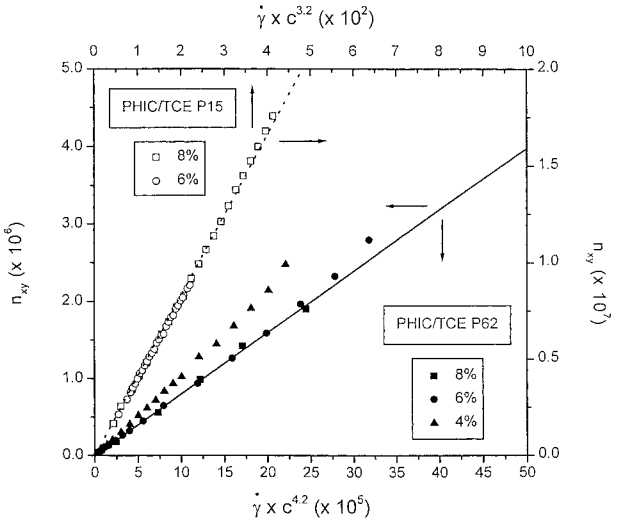

Figure 3. Steady state birefringence $\Delta n'$ sin 2 χ vs $\dot{\gamma}c^{4.2}$ for P15 and P62.

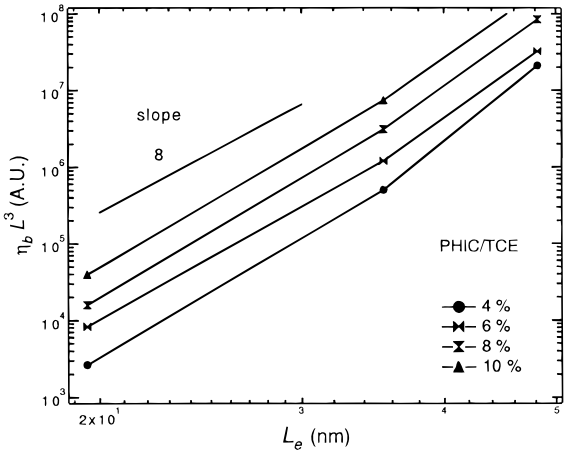

Figure 4. Dependence of $\eta_b L^3$ (in arbitrary units) vs effective length L_e for PHIC/TCE at the indicated concentrations: L_e = 25 nm for $L = \alpha$ = 30 nm. A line with slope = 8 is included for comparison to the data.

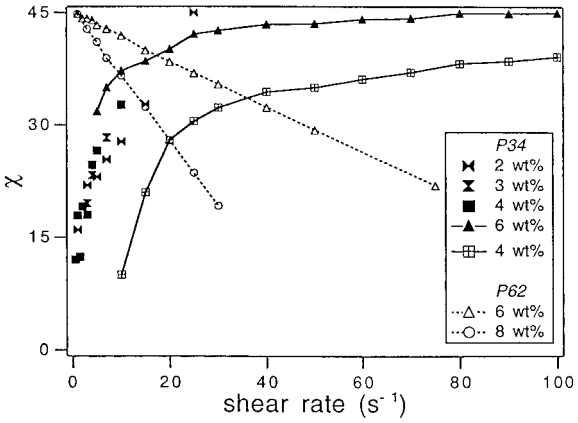

Figure 5. Steady state angle χ as a function of shear rate for P34 and P62 solutions at various shear rates and concentrations. The 4 wt % P34 solution was one day old. The rest of the samples were allowed to equilibrate for 2 weeks.

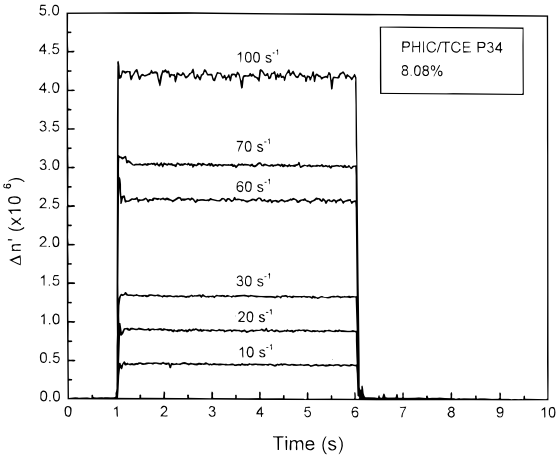

Figure 6. Transient birefringence response in simple shear flow for $c = 8\%$ P34 and various shear rates.

2a. Due to averaging, the analysis at values near the gaps is also affected and the data show some curvature in contrast to the overall linear behavior of the data.

The polymer chains for both P15 and P34 are too short and relax too fast ($\tau < 10$ ms) to exhibit any deviation from Newtonian behavior for the range of shear rates used, and as a result the steady state orientation angle for both samples remained at 45° to the flow direction for all shear rates and concentrations studied, except those for the P34 solutions with $c \leq 6\%$. In these solutions the steady state orientation angle started below 45° for low shear rates and increased toward 45° as shear rate increased (Figure 5). On the other hand, the steady state orientation angle for sample P62 dropped below the 45° with increasing shear rate as normal stresses become important. Fitting Doi−Edwards model[3] to the P62 angle of orientation with the relation $\chi = \arctan(1/\tau\dot{\gamma})/2$, we obtained relaxation times $\tau = 0.014$ s for $c = 6\%$ and $\tau = 0.033$ s for $c = 8\%$.

Transient Birefringence. The P15 as well as the P34 solutions at concentrations above 6% all displayed similar transient behavior. Figure 6 shows a typical time-dependent birefringence response for the 8% solution at various shear rates. The birefringence reaches a steady state value almost immediately after flow starts at $t = 1$ s and rapidly relaxes to zero when the flow is stopped at $t = 6$ s. This simple type of behavior is predicted by the Doi−Edwards constitutive equation for semidilute solutions of rigid rods at shear rates such

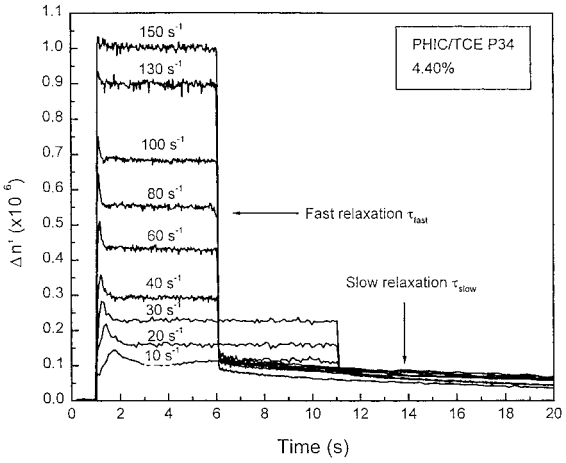

Figure 7. Transient birefringence response for one day old $c = 4.4\%$ P34 and various shear rates.

that $\dot{\gamma}\tau < 1$.[34] The form of the constitutive equation is not expected to change qualitatively when limited flexibility ($L \cong \alpha$) is included, and we will assume that the only effect is that the viscosity is modified as discussed above. In some cases, the data in Figure 6 displayed damped oscillations upon start-up of flow. These oscillations are an artifact and are caused by the mechanical coupling between the motor and the flow cell. The transient response of the orientation angle χ for solutions of P34 and P15 of concentration $c \geq 8$ % is simple. On flow inception, the chains orient at 45°, while, on flow cessation, the chains assume a random orientation thus indicating full relaxation.

An unusual relaxation behavior was observed on flow cessation of moderate to low concentration ($c \leq 6\%$) P34 and P62 solutions. Transient birefringence decay was characterized by two relaxation times (τ_{fast} and τ_{slow}) separated by up to six orders of magnitude. In Figure 7, the transient birefringence for a 4.4% solution of P34 clearly displays a fast mode followed by a very slow mode with $\tau_{slow} \cong 30$ s. The fast mode is similar to the fast relaxation observed in the solutions with $c > 6\%$ and corresponds to rapid reorientation of chains by diffusion. Obviously, the slow mode cannot be attributed to the reorientation of individual chains; it is reasonable to assume that large multichain structures are responsible for the slow relaxation.

The birefringence amplitude of the slow mode $\Delta n'_{slow}$, as measured at the inception of slow mode relaxation, increases slightly with shear rate. Figure 7 also shows that the birefringence overshoots at shear start-up. This overshoot should not be confused with the oscillations caused by the belt in the more concentrated solutions. The time at which the overshoot occurs scales with strain and so is probably associated with orientation by convection of large pre-existing structures in the solution. For samples displaying a slow birefringence mode, the steady state angle is below 45° (Figure 5). The time-dependent orientation angle χ during and after shear is unusual (Figure 8). During shear at the lowest shear rate ($\dot{\gamma} = 10$ s^{-1}) in Figure 8, $\chi \cong 20°$, which is well below the expected value of 45° for molecular orientation when $\dot{\gamma}\tau_{fast} \ll 1$. After flow cessation and fast mode relaxation, the orientation angle assumes an angle close to 0°. This implies that the structures responsible for the slow birefringent mode align along the flow direction. At very long times after flow cessation, orientation becomes random, indicating full relaxation. With increasing shear rate, the steady state χ value increases toward

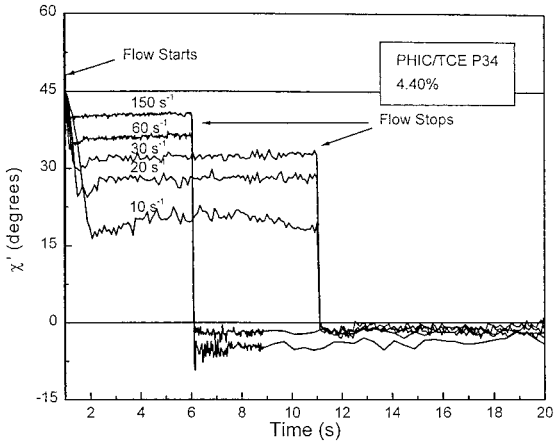

Figure 8. Transient orientation angle for one day old $c = 4.4\%$ P34 and various shear rates.

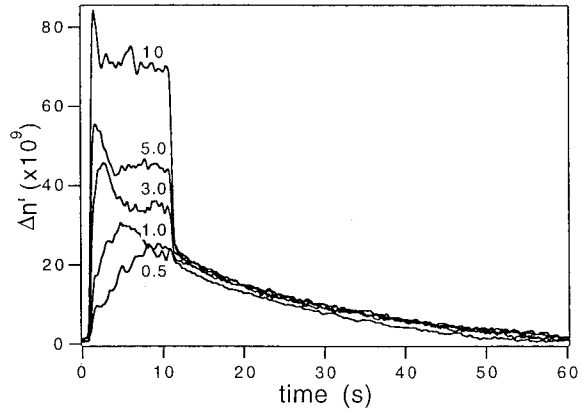

Figure 9. Transient birefringence response for an equilibrated $c = 4\%$ P34 solution; numbers on the graph indicate shear rate in inverse seconds.

45°. Since $\Delta n'_{slow}$ is approximately constant and aligned at $\chi = 0°$, this can be explained by the increasing contribution to the birefringence of the fast mode oriented at 45°. This point will be elaborated later in the paper.

It was found that the magnitude of $\Delta n'_{slow}$ and τ_{slow} decreased with increasing time after sample preparation but stabilized after 1 week. This is the reason for the smaller angle observed in the day old 4.4% solution when compared to the angles for the equilibrated 4% and 6% solutions (Figure 5). Whereas the data presented in Figures 7 and 8 was measured with the 4.4% solution allowed to equilibrate for 1 day, Figure 9 shows the time-dependent birefringence of a 4% P34 solution that was allowed to equilibrate for 2 weeks. $\Delta n'_{slow}$ and τ_{slow} of 2 week old solutions of varying concentration of P34 and P62 were measured (Figure 10). For P34, $\Delta n'_{slow}$ and τ_{slow} initially increase with increasing concentration and reach a maximum near $c = 4\%$ and 6%, respectively. Solutions of P62 similarly displayed two relaxation modes with $\tau_{slow} \cong 35$ s. At higher concentrations, $c \geq 8\%$, τ_{slow} is strongly reduced, and the slow mode becomes essentially unmeasurable by birefringence. The error bars in Figure 10 correspond to the standard deviation obtained by averaging over experiments at different shear rates. For shear rates up to $\dot{\gamma} = 30\ s^{-1}$, no significant shear rate dependence in either $\Delta n'_{slow}$ and τ_{slow} was found. An exception is the slow mode of 6% P34, which decayed with increasing shear rate. No significant effect on the birefringence attributed to the fast mode was found when solutions were

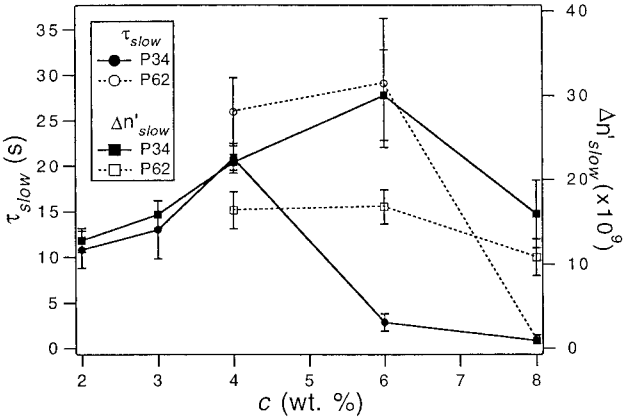

Figure 10. Summary of slow mode relaxation time τ_{slow} and birefringence $\Delta n'_{slow}$ as a function of concentration for equilibrated P34 and P62 solutions.

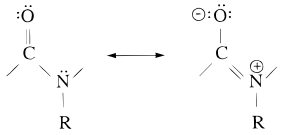

Figure 11. Resonance structures for a PHIC monomer unit.

allowed to equilibrate for different periods of time, thus indicating that the slow mode is caused by relatively weak populations.

Large length scale correlations can be induced by electrostatic interactions in polymer solutions. Usually interactions of this type are stronger at lower concentrations because of longer electrostatic screening lengths. A noteworthy feature of PHIC is the possible formation of resonance structures involving the delocalization of π electrons in the PHIC monomer unit.[36] The resonance structure of the PHIC monomer (Figure 11) results in the polarization of the monomer units along the chain backbone. Due to this sequence of alternating partial charges on each monomer unit, PHIC may display 'polyelectrolyte-like' or 'polyampholyte-like' behavior, as suggested by Goodman and Chen.[63] To investigate any 'polyelectrolyte-like' or 'polyampholyte-like' behavior that may be important in the appearance of the slow mode, several preliminary flow birefringence experiments were conducted with an added organic salt (tetrabutylammonium bromide) that would presumably screen electrostatic interactions. In another set of experiments, solvent polarity was lowered by using toluene instead of TCE. Neither added salt nor less polar solvent resulted in an appreciable change in the slow mode.

One can argue that large structures may be formed by a shear-induced phenomenon. This is however improbable, and the following evidence favors a preexisting structure. First, the slow mode relaxation time lasts much longer than the time for overshoot at shear start-up. Similar time scales for overshoot and relaxation would be expected for flow-induced structures. Second, the slow mode retains a preferred orientation along the flow direction after the flow has stopped and the fast mode has relaxed, (Figure 8). Third, for the 6% P34 and P62 solutions, the slow mode is suppressed by shear: τ_{slow} decreases with increasing shear rate and vanishes at high shear rates, and the condition on flow cessation that $\chi_{slow} = 0°$ also becomes less obvious with increasing shear rate. Multichain structures that would result in the above observations must be optically anisotropic and susceptible to flow alignment. We

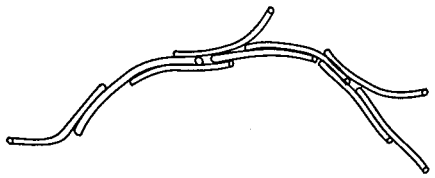

Figure 12. Sketch of possible multichain structure.

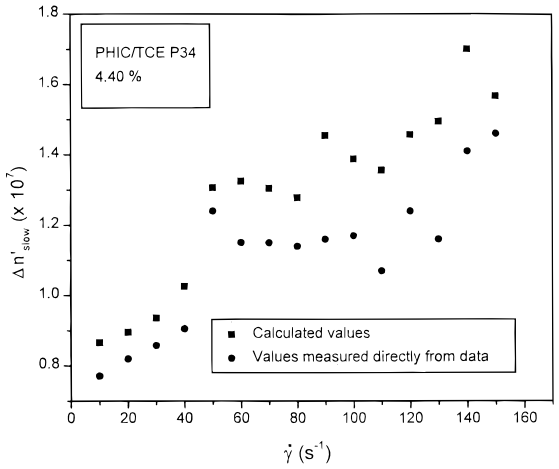

Figure 13. Comparison between the calculated and measured birefringence contributions due to the slow mode $\Delta n'_{slow}$ for one day old 4.4% P34.

therefore postulate the presence of wormlike aggregates consisting of several parallel chains, as depicted Figure 12. We can crudely model the dynamics of these aggregates with a constitutive model such as that developed by Doi and Edwards[3] for entangled rodlike polymers. For $\dot{\gamma}\tau_{slow} > 1$, this model would predict flow alignment as well as overshoots on shear inception. The overshoot may also be due to stretching of multichain wormlike structures. Without further detailed knowledge of the multichain structure and its environment, little more can be said.

Due to the presence of two modes, the birefringence and the orientation angle measurements for the low concentration solutions contain two non-coaxial contributions. It is possible to decouple the two contributions with the following equations:

$$(\Delta n')^2 = (\Delta n'_{fast})^2 + (\Delta n'_{slow})^2 + 2\Delta n'_{fast}\Delta n'_{slow}\cos[2(\chi_{slow} - \chi_{fast})] \quad (14)$$

$$\tan(2\chi) = \frac{\Delta n'_{slow}\sin(2\chi_{slow}) + \Delta n'_{fast}\sin(2\chi_{fast})}{\Delta n'_{slow}\cos(2\chi_{slow}) + \Delta n'_{fast}\cos(2\chi_{fast})} \quad (15)$$

where $\Delta n'$ and χ are the overall measured birefringence and orientation angle, respectively, and $\Delta n'_{fast}$, $\Delta n'_{slow}$, χ_{fast}, and χ_{slow} are the birefringence and orientation angle corresponding to the fast and slow modes. We have seen that the preferred angle for the slow mode is near 0°, while in the low concentration solutions the angle tends to 45° at high shear rates. Moreover, the higher concentration solutions indicate that, in the presence of the fast mode only, the orientation angle remains at 45°. The two contributions to the birefringence can therefore be estimated using eqs 14 and 15 with $\chi_{fast} = 45°$ and χ_{slow} taking the value of χ during slow mode relaxation. In Figure 13 we present the calculated birefringence contribution due to the slow mode $\Delta n'_{slow}$ for the day old 4.4% P34 solution and compare it with

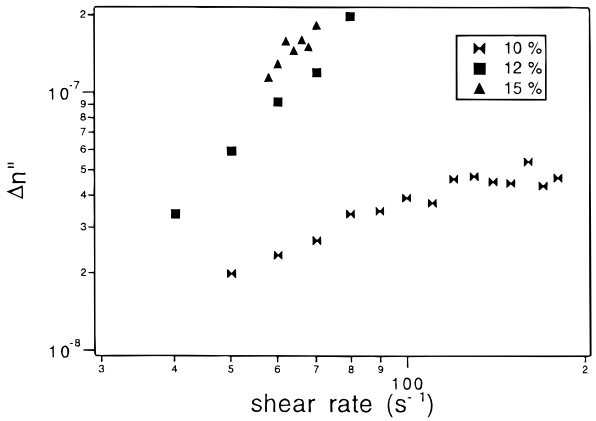

Figure 14. Steady state dichroism $\Delta n''$ as a function of shear rate for P34: $c = 10\%$, 12%, and 15%.

the values obtained by reading the birefringence just after flow cessation, where the fast mode is relaxed and the slow relaxation first becomes evident. The agreement between calculated and measured values reinforces our arguments. The birefringence and viscosity data previously presented in Figures 2−4 in fact show corrected values, so as to include only the contribution from the fast mode. If the overall birefringence is used, the rescaled master curves deviate slightly from the scaling relations for $n_{xy}/\dot{\gamma}$ at low concentrations.

Dichroism. To examine whether the slow mode corresponds to form or scattering contributions to the birefringence, scattering dichroism $\Delta n''$ measurements were performed on all the samples studied. Noticeable dichroism corresponding to the slow mode observed by birefringence could then be attributed to the formation of aggregates with length scales on the order of the wavelength λ. However, only solutions of P34 with $c \geq 10\%$ displayed any noticeable dichroism (Figure 14). In the case of the 10% solution, dichroism approaches a plateau with increasing shear rate while for the 12% solution it increases without any sign of leveling off. It is not clear whether the dichroism is due to large structures related to those responsible for the slow birefringence mode at lower concentrations or whether it may be attributed to a shear-induced structural transition near the isotropic/nematic biphasic regime, which will be the subject of a future study.[64] Since the magnitude of the dichroism is an order of magnitude smaller than the birefringence, the scattering contributions to the birefringence can be assumed to be small.

Dynamic Light Scattering. Dynamic light scattering was used to study the appearance of slow modes in unsheared solutions of PHIC in TCE. At all concentrations studied, the correlation function was dominated by a very slow mode. The *z*-averaged apparent diffusion coefficient $D_{app}(q) = 1/\tau q^2$ was calculated from the relaxation spectrum. As is evident in Figure 15a, D_{app} decreases with increasing concentration and within experimental error appears to be q independent. The apparent hydrodynamic radius $R_H = kT/(6\pi\eta_s D_{app})$ is large and increases with concentration (Figure 15b). Preliminary dynamic light scattering measurements therefore confirm the appearance of large multichain structures that would presumably result in the slow birefringence mode.

DLS measurements were not extended to concentrations above 2 wt %, and so we cannot adequately address the reason for the suppression of the slow birefringence mode at concentrations $c > 6\%$. One

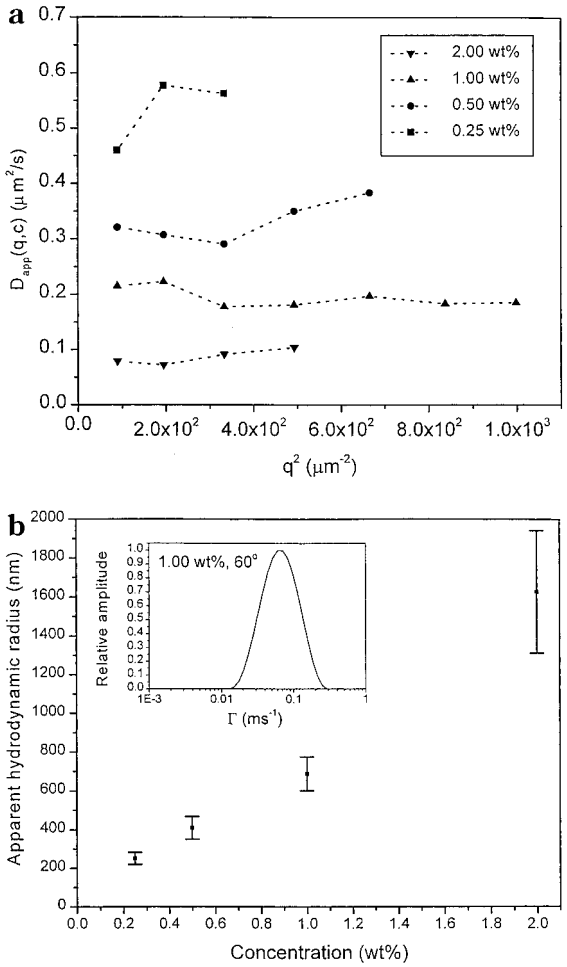

Figure 15. (a) Apparent diffusion coefficient D_{app} of PHIC multichain structures in TCE at various concentrations. (b) Apparent hydrodynamic radius R_H for PHIC multichain structures in TCE as a function of concentration. Inset: Relaxation rate spectrum for 1.0 wt. % measured at $\theta = 60°$.

would expect the amount of aggregation to increase with increasing concentration. However, only those structures that are optically anisotropic and that can be appreciably deformed or oriented are measured by flow birefringence. Increasing aggregation may actually suppress the appearance of a birefringent slow mode if the aspect ratio of resulting structures becomes smaller. Coles *et al.* have shown by dielectric relaxation and electric birefringence experiments that PHIC molecules undergo both linear head-to-tail and antiparallel side-by-side aggregation.[39] At low concentrations, aggregation is predominantly head-to-tail, resulting in linearly aggregated structures of increasing length with increasing concentration. At a critical concentration these linearly aggregated structures attain a maximum length. Above this critical concentration side-by-side aggregation dominates and increases with increasing concentration. This critical concentration was found to decrease with increasing molecular weight. Similar aggregation trends as well as a critical concentration have been observed in PBLG in dioxane.[65] This means that, with increasing concentration, the size of aggregates increases, but at the same time, they become less linear, less orientable by a shear field, and thus less birefringent. To further investigate this mechanism for the apparent suppression of the slow mode, future work will be directed at studies of both polarized and depolarized scattering.

Conclusions

Rheo-optical studies on PHIC solutions with different molecular weights show that steady state birefringence dependence on concentration varies from $n_{xy}/\dot{\gamma} \sim c^{3.2}$ for nearly rodlike chains to $n_{xy}/\dot{\gamma} \sim c^{4.0}$ and $n_{xy}/\dot{\gamma} \sim c^{4.2}$ with increasing molecular weight.

Two distinctive relaxation modes were observed for the low concentration solutions of samples P34 and P62. Dynamic light-scattering measurements in the literature have also revealed two relaxation modes for solutions of rodlike molecules. This is the first time, however, that two modes have been observed rheo-optically. Whereas the fast mode is due to single-chain relaxation, the slow mode is attributed to a multichain structure whose mechanism of formation is not fully understood. We plan to extend these studies to solvents with varying polarity, where aggregation is more or less likely, to other poly(*n*-alkyl isocyanates), and to different molecular architectures, such as three-arm stars.

Acknowledgment. The authors gratefully acknowledge the financial support provided by the NSF/MRSEC program at the University of Massachusetts under Grant NSF/DMR-9400488 and a Faculty Research Grant (FRG) at the University of Massachusetts (UMass). We express our appreciation to Professor Bruce Novak and Nathan Jones at UMass for the preparation and characterization of the PHIC samples. We also acknowledge Chung Yin Kong for assisting with the DLS experiments and thank Professor David Hoagland for use of the DLS apparatus.

References and Notes

(1) de Gennes, P.-G. *Scaling Concepts in Polymer Physics*; Cornell University Press: Ithaca, NY, 1979.
(2) Ferry, J. D. *Viscoelastic Properties of Polymers*, 3rd ed.; Wiley: New York, 1980.
(3) Doi, M.; Edwards, S. F. The Theory of Polymer Dynamics; Oxford University Press: Oxford, 1986.
(4) Larson, R. G. *Constitutive Equations for Polymer Melts and Solutions*; Butterworths: Boston, 1988.
(5) Sato, T.; Teramoto, A. *Macromolecules* **1991**, *24*, 193.
(6) Keep, G. T.; Pecora, R. *Macromolecules* **1988**, *21*, 817.
(7) Zero, K. M.; Pecora, R. *Macromolecules* **1982**, *15*, 87.
(8) Mori, Y.; Ookubo, N.; Hayakawa, R.; Wada, Y. *J. Polym. Sci., Polym. Phys. Ed.* **1982**, *20*, 2111.
(9) Odijk, T. *Macromolecules* **1983**, *16*, 340.
(10) Doi, M. *J. Polym. Sci., Polym. Symp.* **1985**, *73*, 93.
(11) Semenov, A. *J. Chem. Doc., Faraday Trans. 2* **1986**, *82*, 317.
(12) Sato, T.; Takada, Y.; Teramoto, A. *Macromolecules* **1991**, *24*, 6220.
(13) Berry, G. C. *J. Rheol.* **1996**, *40*, 1129.
(14) Shukla, P.; Muthukumar, M.; Langley, K. H. *J. Appl. Polym. Sci.* **1992**, *44*, 2115.
(15) Tinland, B.; Maret, G.; Rinaudo, M. *Macromolecules* **1990**, *23*, 596.
(16) Milas, M.; Rinaudo, M.; Knipper, M.; Schuppiser, J. L. *Macromolecules* **1990**, *23*, 2506.
(17) Takada, Y.; Sato, T.; Teramoto, A. *Macromolecules* **1991**, *24*, 6215.
(18) Fouissac, E.; Milas, M.; Rinaudo, M. *Macromolecules* **1993**, *26*, 6945.
(19) Milas, M.; Roure, I.; Berry, G. C. *J. Rheol.* **1996**, *40*, 1155.
(20) Ohshima, A.; Kudo, H.; Sato, T.; Teramoto, A. *Macromolecules* **1995**, *28*, 6095.
(21) Yamaguchi, M.; Wakutsu, M.; Takahashi, Y.; Noda, I. *Macromolecules* **1992**, *25*, 470.
(22) Rubingh, D. N.; Yu, H. *Macromolecules* **1976**, *9*, 681.
(23) Murakami, H.; Norisuye, T.; Fujita, H. *Macromolecules* **1980**, *13*, 145.
(24) Itou, T.; Chikiri, H.; Teramoto, A.; Aharoni, S. M. *Polym. J.* **1988**, *20*, 143.
(25) Yu, M.; Liu, Q. *Macromolecules* **1996**, *29*, 6928.
(26) Wang, H.; DuPre, D. B. *J. Chem. Phys.* **1991**, *96*, 1523.
(27) Jinbo, Y.; Sato, T.; Teramoto, A. *Macromolecules* **1994**, *27*, 6080.

(28) Berger, M. N.; Tidswell, B. M. *J. Polym. Sci., Polym. Symp.* **1973**, *42*, 1063.
(29) Conio, G.; Bianchi, E.; Cifferri, A.; Krigbaum, W. R. *Macromolecules* **1984**, *17*, 856.
(30) Kuwata, M.; Murakami, H.; Norisuye, T.; Fujita, H. *Macromolecules* **1984**, *17*, 2731.
(31) Takada, S.; Itou, T.; Chikiri, H.; Einaga, Y.; Teramoto, A. *Macromolecules* **1989**, *22*, 973.
(32) Yamakawa, H.; Yoshisaki, T. *J. Chem. Phys.* **1981**, *75*, 1016. Yamakawa, H.; Yoshisaki, T.; Shimada, J. *J. Chem. Phys.* **1983**, *78*, 560. Yamakawa, H.; Yoshisaki, T. *J. Chem. Phys.* **1983**, *78*, 572.
(33) Bur, A. J.; Roberts, D. E. *J. Chem. Phys.* **1969**, *52*, 406.
(34) Bur, A. J.; Fetters, L. *J. Chem. Rev.* **1976**, *76*, 727.
(35) Itou, T.; Teramoto, A. *Macromolecules* **1988**, *21*, 2225.
(36) Cook, R.; Johnson, R. D.; Wade, C. G.; O'Leary, D. J.; Munoz, B.; Green, M. M. *Macromolecules* **1990**, *23*, 3454.
(37) Chow, A. W.; Fuller, G. G.; Wallace, D. G.; Madri, J. A. *Macromolecules* **1985**, *18*, 786.
(38) Yu, H.; Bur, A. J.; Fetters, L. J. *J. Chem. Phys.* **1966**, *44*, 2568.
(39) Coles, H. J.; Gupta, A. K.; Marcal, E. *Macromolecules* **1977**, *10*, 182.
(40) Patten, T. E.; Novak, B. M. *J. Am. Chem. Soc.* **1991**, *113*, 5065.
(41) Fulmer, A. W.; Bensbasat, J. A.; Bloomfield, V. A. *Biopolymers* **1981**, *20*, 1147.
(42) Ferrari, M. E.; Bloomfield, V. A. *Macromolecules* **1992**, *25*, 5266.
(43) Weissenburg, P.; Odijk, T.; Cirkel, P.; Mandel, M. *Macromolecules* **1995**, *28*, 2315.
(44) Richtering, W.; Gleim, W.; Burchard, W. *Macromolecules* **1992**, *25*, 3795.
(45) Petekidis, G.; Vlassopoulos, D.; Fytas, G.; Kountourakis, N. *Macromolecules* **1997**, *30*, 919.
(46) Southwick, J. G.; Jamieson, A. M.; Blackwell, J. *Macromolecules* **1981**, *14*, 1728.
(47) Odijk, T. *Macromolecules* **1994**, *27*, 4998.
(48) Mattoussi, H.; Karasz, F. E.; Langley, K. H. *J. Chem. Phys.* **1990**, *93*, 3593.
(49) Sedlak, M.; Amis, E. J. *J. Chem. Phys.* **1992**, *96*, 826.
(50) Sedlak, M. *J. Chem. Phys.* **1994**, *101*, 10139.
(51) Walkenhorst, R.; Dorfmuller, T.; Eimer, W. *Ber. Bunsen-Ges. Phys. Chem.* **1995**, *99*, 137.
(52) Sedlak, M. *J. Chem. Phys.* **1996**, *105*, 10123.
(53) Aharoni, S. M. *Macromolecules* **1979**, *12*, 94. Aharoni, S. M. *Polym. Bull.* **1981**, *5*, 95.
(54) Aharoni, S. M.; Walsh, E. K. *Macromolecules* **1979**, *12*, 271.
(55) Doi, M.; Edwards, S. F. *J. Chem. Soc., Faraday Trans. 2* **1978**, *74*, 560. Doi, M.; Edwards, S. F. *J. Chem. Soc., Faraday Trans. 2* **1978**, *74*, 918.
(56) Fuller, G. G. *Optical Rheometry of Complex Fluids*; Oxford University Press: Oxford, 1995.
(57) de Gennes, P.-G. *Macromolecules* **1976**, *9*, 587 and 594.
(58) Goodwin, A.; Novak, B. M. *Macromolecules* **1994**, *27*, 5520.
(59) Schneider, N. S.; Furusaki, S.; Lenz, R. W. *J. Polym. Sci. A* **1965**, *3*, 933.
(60) Kalogrianitis, S. G.; van Egmond, J. W. *J. Rheol.* **1997**, *41*, 343.
(61) Stepanek, P. In *Dynamic Light Scattering*; Brown, W., Ed.; Oxford University Press: Oxford, 1993.
(62) Provencher, S. W. *Comput. Phys. Commun.* **1982**, *27*, 213 and 229.
(63) Goodman, M.; Chen, S. *Macromolecules* **1970**, *3*, 398.
(64) Gatzonis, Y.; van Egmond, J. W. In preparation.
(65) Gupta, A. K.; Dufour, C.; Marchal, E. *Biopolymers* **1974**, *13*, 1293. Gupta, A. K. *Biopolymers* **1976**, *8*, 1543.

MA9618540